Building KCNQ1/KCNE1 Channel Models and Probing their Interactions by Molecular-Dynamics Simulations

Yu Xu, Yuhong Wang, Xuan-Yu Meng, Mei Zhang, Min Jiang, Meng Cui, and Gea-Ny Tseng*

Department of Physiology & Biophysics, Virginia Commonwealth University, Richmond, Virginia

Submitted August 2, 2013, and accepted for publication September 11, 2013.

*Correspondence: gtseng@vcu.edu

Editor: Randall Rasmusson.

Yu Xu, Yuhong Wang, and Yuan-Yu Meng contributed equally to the article.

SUPPLEMENTAL DATA

A Detailed methods

Molecular biology and side-directed mutagenesis

KCNQ1 was in vector pcDNA3.1/V5-His-TOPO (Invitrogen, for COS-7 expression) or pSP64 (Promega, for oocyte expression). KCNE1 was in pAlterMax (Promega, for both COS-7 and oocyte expression). For both, two versions were used: wild-type (WT) and Cys-free (all native Cys replaced Ala, labeled as Q1* and E1*). Mutations were created using the QuickChange mutagenesis kit (Invitrogen). All were confirmed by direct DNA sequencing. For *in vitro* transcription, linearized plasmids were transcribed using SP6 or T7 RNA polymerase and commercial kits (Mmessage Mmachine, Ambion, TX).

Oocyte expression and voltage clamp experiments

These experiments have been described in details previously (1). Whole oocyte currents were recorded using the '2-cushion pipette' voltage clamp method. During recordings, oocyte was continuously superfused with a low-Cl ND96 solution to reduce interference from endogenous Cl channels. Voltage clamp was done at room temperature (24-26^{o}C) with OC-725B or OC-725C amplifier (Warner Instruments, MA). Voltage clamp protocol generation and data acquisition were controlled by pClamp 10 via DigiData 1440A interface (Molecular Devices). Currents were low-pass filtered at 1 kHz (Frequency Devices, MA). Voltage clamp protocols are described in figures.

COS-7 expression and immunoblot experiments

These experiments have been described in details previously (1). To detect disulfide bond formation using non-reducing immunoblots, COS-7 cells were incubated in 20 mM N-ethylmaleimide (NEM) for 10 min to protect free thiol groups before making whole cell lysate (WCL). WCLs were fractionated by non-reducing SDS polyacrylamide gels and after blotting, the membrane was probed for KCNQ1 or KCNE1 with suitable primary and secondary Abs. Immunoreactivity was visualized using an ECL detection kit (Amersham), and band intensities were quantified by densitometry.

Docking the KCNE1 N-terminal domain (E1-NT) to the structure of KCNE1 transmembrane domain docked to the KCNQ1 homology model: $(Q1)_4$/(E1-TMD)

The flow charts in Fig. S4, panels A and B, list the procedures.

The only experimental data that suggest a preferred spatial relationship between E1-NT and the Q1 channel are from Morin and Kobertz (2). These investigators modified charybdotoxin (ChTx) by mutating Arg at position 19 (on the backside of ChTx, with reference to its interaction surface) to Cys and conjugate the R19C side chain with a bismaleimide cross-linker (Mal). When they applied ChTx-Mal to $Q1^S$/E1-Cys channel complexes, in which $Q1^S$ was a Q1 mutant with high ChTx affinity (3) and E1-Cys had a Cys engineered into one of several positions in the E1-NT region, they found a position-dependent reactivity with ChTx-Mal: T14C (100%), Q22C (40%), and S34C (90%) (W. R. Kobertz, personal communication). Importantly, when there was an unmodified ChTx bound to the pore entrance, free ChTx-Mal molecules in the bath solution could not react with E1-T14C. These data suggested that the extent of the reaction between the target Cys on E1-NT and ChTx-Mal was dependent on the length of the bismaleimide cross-linker.

To take advantage of these observations, we first created a ChTx/$(Q1^S)_4$ conformation (panel B in Fig. S4). This was made possible by the ChTx/$KcsA^S$ NMR structure (4) (2A9H.pdb), in which $KcsA^S$ is a KcsA mutant of high ChTx affinity. Below is sequence alignment in the pore region between wild-type KcsA and Q1, and their ChTx-sensitive variants ($KcsA^S$ and $Q1^S$, respectively). Yellow shading indicates mutations or deletions introduced to confer a high ChTx binding affinity. Pore-loop residues are underlined.

```
KcsA-WT       LAERGAPGAQLITYPRALWWSVETATTVGYGDLYPVTLWGR
KcsA^S        LAERGAPGAALISYPDALWWSVETATTVGYGDLYPVTLWGR
KCNQ1^S       DAVNS----GFGSYADALWWGVVTVTTIGYGDIVPVTWVGK
KCNQ1-WT      DAVNESGRVEFGSYADALWWGVVTVTTIGYGDKVPQTWVGK
```

We modified the Q1 homology model to $Q1^S$, and refined it by energy minimization using SYBYL. We then replaced the $KcsA^S$ in 2A9H with $Q1^S$ (based on the high sequence homology in the pore region, above), and refined the ChTx/$(Q1^S)_4$ structure by energy minimization (panel C in Fig. S4). We checked the expected contacts between ChTx and $Q1^S$ in the docking conformation (table). First and second columns list the contacts between ChTx and $KcsA^S$ (with chain ID) in 2A9H.pdb. Third column lists the $Q1^S$ residues (shown for wild-type residues, position numbers and, when applicable, mutated residue in parenthesis) that are expected to make contacts with the ChTx residues listed in the first column. Fourth column lists the C_α-C_α distances between ChTx and $Q1^S$ residues in our ChTx/$(Q1^S)_4$ model.

ChTx	$KcsA^S$	$KCNQ1^S$	Cα-Cα dist (Å)
F2	L81/*d*	K318(I)	9.92
K11	D64/*b*	D301	10.12
W14	V84/*c*	Q321(V)	9.40
R25	L81/*c*	K318(I)	7.19
R25	D64/*c*	D301	11.53
M29	Y82/*a*	V319(Y)	7.02
N30	L81/*a*	K318(I)	5.53
Y36	A58/*d*	E295(G)	10.35
Y36	Y82/*d*	V319(Y)	9.65
S37	V84/*d*	Q321(V)	8.44

We then replaced $(Q1)_4$ in the 30,254 early docking conformations of $(Q1)_4$/$(E1\text{-}TMD)_4$/(E1-NT) (flow chart in Fig. S4, panel A) with ChTx/$(Q1^S)_4$ to create ChTx/$(Q1^S)_4$/$(E1\text{-}TMD)_4$/(E1-NT) conformations. Among these conformations, we selected those with < 18 Å C_α-C_α distances between E1 positions 14 and 34 and ChTx position 19 (filter 1 in flow chart of Fig. S4, panel A). The value of 18 Å was based on the estimated length of a fully-extended Mal linker. Note that because we had only one E1-NT in these conformations, its relationship with ChTx bound to the $Q1^S$ external pore entrance would depend on the ChTx orientation. Therefore, for each of the E1-NT conformations, we examined the distances between E1 positions 14 and 34 and ChTx position 19 in 4 different ChTx orientations, i.e. rotating ChTx in ChTx/$(Q1^S)_4$/$(E1\text{-}TMD)_4$/(E1-NT) by 90°, 180°, and 270° while maintaining the ChTx/$Q1^S$ contacts. This selection drastically reduced the number of possible conformations to 916.

Among these conformations, we removed those having clashes between E1-NT and the bound ChTx, and those structures similar to each other (filters 2 and 3 in Fig. S4, panel A). After this selection, 22 distinct conformations remain that have > 3.5 Å RMSD between their C_α atoms. Panel D in Fig. S4 compares these 22 conformations. For better clarity, we hide the ChTx structure and superimpose the highly similar $(Q1^S)_4$/$(E1\text{-}TMD)_4$ structures. When viewed from the extracellular side of the membrane, the 22 docked E1-NT structures (each represented by a distinct color) show a clear preference for one or the other VSD-PD interface (marked as regions 1 and 2). Furthermore, these 22 docked E1-NT structures could be roughly classified as having their helices (aa 11-23) facing toward, or away from, the external surface of the Q1 channel. These two configurations are called 'Ea' and 'Eb'. We inspected each of these 22 structures to remove those violating modeling criteria (filter 4). After careful inspection, 4 structures remained: 2 had the Ea conformation in region 2, and 2 had the Eb conformation in region 1. We selected one from each type of conformation for further analysis. We built the loop connecting aa 34 and 40, so that E1-TMD and E1-NT became connected (as E1-TMD-NT). We removed ChTx and the extra E1-TMD, replaced $Q1^S$ with wild-type Q1, and duplicated the E1-TMD-NT. This created 2 docking conformations of $(Q1)_4$/$(E1\text{-}TMD\text{-}NT)_2$: Q1/Ea and Q1/Eb, that were subjected to MD simulations under 2 conditions as described in the main text.

B Figure and video legends

Fig. S1 Negative controls for Q1*-L142C/R228C. Fig. 2B in the main text shows that Q1*-L142C/R228C manifested a prominent constitutive component, which was abolished by DTT treatment. This led us to propose that 142C and 228C formed a disulfide bond in the open state, and the disulfide-bonded form stabilized the Q1*-L142C/R228C channel in the open state. As negative controls, we

expressed Q1*-L142C and Q1*-R228C separately, and tested whether DTT treatment could affect their gating kinetics or voltage-dependence of activation. **(A)** Q1*-L142C expressed alone was not sensitive to DTT in either gating kinetics or voltage-dependence of activation. **(B)** Q1*-R228C expressed alone produced too little current for analysis. Coexpressing E1-WT with Q1*-R228C increased the current amplitude, which was insensitive to DTT in either gating kinetics (right) or voltage-dependence of activation (left). To confirm that the current was mediated by E1-WT/Q1*-R228C, instead of E1-WT/oocyte Q1, the right panel shows that MTSES (5 mM) treatment induced a large constitutive current due to stabilization of the S4 voltage sensor in the 'UP' position (similar to the effects of MTSET on KCNQ1-R228C reported previously (5)). MTSES had no such effect on E1-WT/oocyte Q1 (data not shown).

Fig. S2 Trajectories of root-mean-square-deviation (RMSD) of C_α atoms of manually adjusted KCNE1 NMR structure during 100-ns MD simulation. The RMSD values for full-length E1 and separate E1 regions (aa numbers and color codes depicted in 'B') are reported. Gray shading highlights 50-100 ns of MD run during which the poses were subjected to cluster analysis.

Fig. S3 Flow chart of docking KCNE1 TMD to KCNQ1 homology model. Model selection (filters 2-5) was based on data from disulfide trapping experiments (6-11).

Fig. S4 Flow chart of docking KCNE1 NT to $(Q1)_4$/(E1-TMD). (A) Flow chart of docking E1-NT to $(Q1)_4$/(E1-TMD) and, after a series of filters, creating two versions of the $(Q1)_4$/(E1-TMD-NT)$_2$ docking conformation. **(B)** Flow chart of creating ChTx/$(Q1^S)_4$. **(C)** Top view of ChTx/$(Q1^S)_4$ with key ChTx and Q1 residues that made contact with each other highlighted in space-filled format. **(D)** Top view of the 22 superimposed E1-NT structures docked to $(Q1)_4$/(E1-TMD), obtained after filter 3 in the flow chart, panel A. More details of the docking and selecting procedures are provided in the text of on-line Supplemental Data.

Fig. S5 (A) – (B) Complete IB images from the same experiments as shown in Fig. 5A. **(C)** Summary of densitometry quantification. (n): numbers of independent COS-7 expression/immunoblot experiments. Note that the disulfide-linked Q1*-E290C/E1-R33C band appeared stronger after 100 mM [K] treatment, consistent with an open-state preference of disulfide formation. However, Fig. 8 in the main text shows that H_2O_2 treatment shifted the voltage-dependence of Q1*-E290C/E1-R33C activation in the positive direction, suggesting that disulfide formation stabilized the channel in a closed (pre-open) state. The interaction between Q1*-E290 and E1-R33 was predicted by both Q1Ea and Q1Eb docking conformations, unlike 7 other tested KCNQ1-KCNE1 interactions that were predicted by either Q1Ea or Q1Eb, but not both (Fig. 5, top diagram; Table S1). It is possible that the cell surface KCNQ1/KCNE1 channels were more dynamic when incubated in 100 mM [K] (membrane depolarization) than in 5 mM [K] (no depolarization). This allowed the KCNE1 NT domain to explore a wider conformational space and adopt both Q1Ea and Q1Eb configurations at different times. This then trapped Q1*-290C and E1-33C in disulfide-bonded state to a higher degree, although the encounter occurred in the pre-open activated state of the channel.

Fig. S6 (A) and (C) Complete IB images from the same experiments as shown in Fig. 5B and 5C. **(B)** Densitometry of immunoblot experiments shown in (A).

Fig. S7 Testing whether KCNE1 position 58 is close enough to KCNQ1 positions 338, 339, or 340 to allow disulfide bond formation. (A) Probing disulfide bond formation between KCNE1 position 57, 58 or 59, and KCNQ1 position 338, 339 or 340. All these Cys-substituted mutants were made in native Cys-removed background (E1* and Q1*). WCLs from COS-7 cells expressing E1* and Q1* variants were divided into 2 aliquots, one treated with DTT while the other not. WCLs were fractionated by non-reducing SDS-PAGE, and probed for Q1 (top) and E1 (bottom). E1*-40C/Q1*-147C was included as positive control. **(B)** Validating the experimental conditions used to detect disulfide formation between KCNQ1 and KCNE subunit in the extracellular juxtamembrane region (between Q1*-Q147C and E1-

G40C) (9) and in the transmembrane region (between Q1*-331C and E2-M59C) (1). The experimental conditions were described previously. Samples were fractionated by non-reducing SDS gel electrophoresis and analyzed by immunoblotting (IB) with Q1-targeting Ab. Q1 monomer, $(Q1)_1$, migrates as a 60 kDa band. Disulfide-linked Q1*-331C/E2-M59C migrated as a prominent band just above the 150 kDa marker, that was abolished by DTT treatment. The size predicts disulfide-linked Q1/E2 dimer, $(Q1/E2)_2$. Disulfide-linked Q1*-Q147C/E1-G40C migrated as an 80 kDa, that was abolished by DTT treatment. The sizes correspond to disulfide-linked Q1/E1 monomer '$(Q1/E1)_1$', with different degrees of E1 glycosylation (9). In rare cases (as is shown here), disulfide-linked Q1*-Q147C/E1-G40C also had a disulfide-linked Q1/E2 dimer, $(Q1/E2)_2$, band. **(C)** Summary of ratios of intensity of $(Q1/Ex)_Y$ or $(Q1)_n$ bands (X and Y = 1 or 2) to $(Q1)_1$ band, without (red circles) or with (blue triangles) DTT treatment. cDNAs are listed on top. (n): number of independent experiments.

Fig. S8 KCNQ1 and KCNE1 interactions based on molecular dynamics simulation under condition #2 (nominally ion free, 0 mV). (A) *a*: KCNE1 C_α RMSF values during 50-100 ns MD simulations of E1 alone, Q1Ea and Q1Eb. *b*: Degree of KCNE1 contacts with KCNQ1 indexed by KCNE1 position number. Quantification of Q1/E1 contacts was the same as described for Fig. 6B, and the values were averaged from Q1Ea and Q1Eb. *c*: KCNQ1 regions with which KCNE1 was making contact during MDS#2, averaged from Q1Ea and Q1Eb. **(B)** *a*: KCNQ1 C_α RMSF values during 50-100 ns MD simulations of Q1 alone, Q1Ea and Q1Eb. b: Degree of KCNQ1 contacts with KCNE1 indexed by KCNQ1 position number. Quantification of Q1/E1 contacts was the same as described for Fig. 7B, and the values were averaged from Q1Ea and Q1Eb.

Fig. S9 Principal component analysis of Q1 backbone motions in Q1 alone vs Q1 with E1 associated in Q1Ea or Q1Eb conformation (Q1-to-Q1Ea and Q1-to-Q1Eb, respectively). The equilibrium phase (50-100 ns) of MD trajectory of Q1 alone was combined with that of Q1Ea or Q1Eb. The covariance matrices of the combined trajectories were diagonalized, generating eigen vectors and corresponding eigen values that described the directions and magnitudes of different principal components of collective motions in Q1 backbone during the combined trajectories. These principal components were ranked by their eigen values of descending order, so that principal component 1 had the largest eigen value (i.e. the largest magnitude of collective motions). **(A)** Contributions of the first 10 principal components to molecular motions in the combined Q1-to-Q1Ea and Q1-to-Q1Eb trajectories. **(B)** Cross plots of projections on eigen vector 1 (abscissa) and eigen vector 2 (ordinate) for Q1 alone or Q1Ea in their combined trajectories (top), and for Q1 or Q1Eb in their combined trajectories (bottom). The paths of trajectories are signified by gray (Q1 alone), red (Q1Ea) and blue (Q1Eb) lines, with the initial positions signified by the yellow circles or triangles. **(C)** Cross plots of projections on eigen vector 2 and 3 for Q1-to-Q1Ea or Q1-to-Q1Eb. The analysis was performed using GROMACS based on MDS#1.

Fig. S10 Q1 C_α motions induced by E1 association in Q1Ea and Q1Eb conformations based on MDS#1 (top) and MDS#2 (bottom). In all panels, Q1 backbones are shown as gray traces and the regions of interest (ROIs, marked on top) are highlighted as white tubes. These correspond to the initial Q1 C_α positions of the first principal components (PC1), which describe the E1-induced Q1 motions under the 4 sets of conditions (marked on the left). The directions and magnitudes of these motions are signified by the blue-green-red lines extended from the C_α atoms in ROIs: for each of the C_α atoms, the 'blue' and 'red' ends of the line indicate its initial and end positions along PC1. Each of the Q1Ea and Q1Eb complexes has two E1 subunits associated with one Q1 tetramer channel. They are signified by the purple and yellow ellipses in the columns for S3-S4 linker from the extracellular view and S4-S5 linker from the intracellular view.

Fig. S11 Enlarged views of Fig. 7D. See Fig. 7D legend for details.

Fig. S12 Cartoons depicting the network of salt-bridge and hydrogen-bond interactions between charged or hydrophilic side chains in different regions of Q1 and between Q1 and E1 in Q1Ea and Q1Eb docking conformations, based on data in Table S1.

Fig. S13 (A) *Top*: Fluctuations in pore dimensions of Q1 alone, Q1Ea and Q1Eb during MDS#2. Eleven poses each of Q1, Q1Ea and Q1Eb taken from 100 ns MD trajectories at 10 ns intervals were subjected to analysis by the program 'Hole' (12). Q1 positions along the pore central (z) axis were aligned based on C_α position of T312 (defined as zero, with positive z-axis values toward the extracellular side and negative z-axis values toward the intracellular side of the membrane). This allowed us to average the estimated pore radii over the 11 poses. Shown are mean$\pm$SE values of pore radii of Q1, Q1Ea and Q1Eb, with selected C_α positions marked along the abscissa. **(B)** As a reference, we applied the same type of analysis to crystal structures of K channels in closed state (KcsA: 1K4C.pdb, KvLm: 4H33,pdb) or in open state (Kv1.2_Kv2.1 chimera: 2R9R.pdb, MthK: 3DLC.pdb). Their pore radii were aligned by the selectivity filter (TVGYGD, C_α positions marked by dots along the abscissa, using the same color codes as the curves of pore radii). Based on the pore radii of crystal structures, we specified the selectivity filter, (inner) cavity, and (activation or $S6_{CT}$) gate of Q1, Q1Ea and Q1Eb. Note that the gate was in the open state in Q1, but switched to the closed state in Q1Ea and Q1Eb, and the P343 hinge was at the transition between 'cavity' and 'gate'. Although the 4 K channel crystal structures manifested well-defined narrower regions in the selectivity filter, corresponding to K^+ binding sites coordinated by peptide backbone carbonyl oxygens protruding into the pore lumen, such features were not obvious in the Q1, Q1Ea or Q1Eb pore, reflecting the dynamic nature of the peptide backbones during MD trajectories. **(B)** Superimposed side views (of single subunits S5-P loop-S6, rotating 90^o as indicated) and bottom views (4 subunits) of selected poses of Q1, Q1Ea and Q1Eb. In Q1Ea and Q1Eb but not Q1, S6 kinked at P343 (but not A366), causing the $S6_{CT}$ to bend toward the pore central axis (side views) and reducing the opening of the intracellular pore entrance (bottom views).

Animation shows the following sequence: (1) KCNQ1 alone, rotation to show top and side 3-D views, with S1 to S6 of one subunit highlighted by different colors, (2) Q1Ea binding conformation, rotation to show side and top views, (3) principal component 1 of Q1 C_α motions induced by E1 binding in the Q1Ea conformation, illustrated by Q1 C_α ribbon morphed from Q1 alone to Q1Ea, top and under views (from the extracellular and intracellular side of the membrane, respectively), (4) Q1Eb binding conformation (details similar to '2' above), and (5) principal component 1 of Q1 C_α motions induced by E1 binding in the Q1Eb conformation (details similar to '3' above).

C References

1. Wang, Y.-H., M. Zhang, Y. Xu, M. Jiang, D. P. Zankov, M. Cui, and G.-N. Tseng. 2012. Probing the structural basis for differential KCNQ1 modulation by KCNE1 and KCNE2. J Gen Physiol. 140: 653-669.
2. Morin, T. J. and W. R. Kobertz. 2008. Counting membrane-embedded KCNE β-subunits in functioning K^+ channel complexes. PNAS. 105: 1478-1482.
3. Chen, H., L. A. Kim, S. Rajan, S. Xu, and S. A. N. Goldstein. 2003. Charybdotoxin binding in the I_{Ks} pore demonstrates two minK subunits in each channel complex . Neuron. 40: 15-23.
4. Yu, L., C. Sun, D. Song, J. Shen, N. Xu, A. Gunasekera, P. J. Hajduk, and E. T. Olejniczak. 2005. Nuclear magnetic resonance structural studies of a potassium channel-charybdotoxin complex. Biochemistry. 44: 15834-15841.
5. Rocheleau, J. M. and W. R. Kobertz. 2008. KCNE peptides differently affect voltage sensor equilibrium and equilibration rates in KCNQ1 K^+ channels. J Gen Physiol. 131: 59-68.
6. Tapper, A. R. and A. L. Jr. George. 2001. Location and orientation of minK within the I_{Ks} potassium channel complex. J Biol Chem. 276: 38249-38254.
7. Nakajo, K. and Y. Kubo. 2007. KCNE1 and KCNE3 stabilize and/or slow voltage sensing S4 segment of KCNQ1 channel. J Gen Physiol. 130: 269-281.

8. Xu, X.-L., M. Jiang, K.-L. Hsu, M. Zhang, and G.-N. Tseng. 2008. KCNQ1 and KCNE1 in the I_{Ks} channel complex make state-dependent contacts in their extracellular domains. J Gen Physiol. 131: 589-603.
9. Wang, Y.-H., M. Jiang, X.-L. Xu, K.-L. Hsu, M. Zhang, and G.-N. Tseng. 2011. Gating-related molecular motions in the extracellular domain of the I_{Ks} channel: implications for I_{Ks} channelopathy. J Memb Biol. 239: 137-156.
10. Chung, D. Y., P. J. Chan, J. R. Bankston, L. Yang, G. Liu, S. O. Marx, A. Karlin, and R. S. Kass. 2009. Location of KCNE1 relative to KCNQ1 in the I_{Ks} potassium channel by disulfide cross-linking of substituted cysteins. PNAS. 106: 743-748.
11. Chan, P. J., J. D. Osteen, D. Xiong, M. S. Bohnen, D. Doshi, K. J. Sampson, S. O. Marx, A. Karlin, and R. S. Kass. 2012. Characterization of KCNQ1 atrial fibrillation mutations reveals distinct dependence on KCNE1. J Gen Physiol. 139: 135-144.
12. Smart, O. S., J. G. Neduvelil, X. Wang, B. A. Wallace, and M. S. P. Sansom. 1996. HOLE: a progam for the analysis of the pore dimensions of ion channel structural models. Journal of Molecular Graphics. 14: 354-360.

TABLE S1 Salt-bridge and H-bond interactions between KCNQ1 domains and between KCNQ1 and KCNE1 observed during MD simulations of Q1 alone, Q1/Ea, and Q1/Eb, under two conditions (MDS#1[a] & MDS#2[b])

				Q1-Q1 interactions									Q1-E1 interactions			
				Q1 alone		Q1/Ea		Q1/Eb					Q1/Ea		Q1/Eb	
				Frequency[f]		Frequency[f]		Frequency[f]					Frequency[f]		Frequency[f]	
Q1 domain_1[c]	Q1 residue_1[c]	Q1 residue_2[d]	Q1 domain_2[d]	MDS1	MDS2	MDS1	MDS2	MDS1	MDS2	Q1 residue	E1 residue[e]	E1 domain[e]	MDS1	MDS2	MDS1	MDS2
S-1S2 linker	E146	R228	S4	0.28	0.33	0.25	0.04	0.03	0.23							
		R231	S4	0.99	0.46	0.43	0.74	0.52	0.41							
		R293	S5-P linker	0.71	0.00	0.06	0.00	0.29	0							
	Q147	R228	S4	0.71	0.3575	0.06	0.195	0.29	0	Q147	D39	NT	0.115	0	0	0
		R231	S4	0	0.1525	0	0.0975	0.08	0		R32	NT	0	0	0	0.545
		E284	S5-P linker	0.32	0.05	0.00	0.03	0.15	0.023							
		N289	S5-P linker	0.00	0.12	0.12	0.00	0.01	0.05							
		E290	S5-P linker	0.01	0.00	0.14	0.00	0.00	0.005							
		R293	S5-P linker	0.15	0.00	0.00	0.01	0.01	0							
S2 helix	E160	R231	S4	0.12	0.48	0.28	0.30	0.09	0.71							
		Q234	S4	0.81	1.00	0.90	1.00	0.87	1							
		R237	S4	0.96	0.58	0.80	0.79	0.92	0.37							
	E170	R174	S4	0.8625	0.923	0.8375	0.645	0.77	0.825							
		R237	S4	0	0	0	0.003	0	0.125							
		H240	S4	0.07	0.688	0.2625	0.61	0.19	0.19							
		R243	S4	0.335	0.463	0.21	0.395	0.2925	0.465							
		Q244	S4	0.64	0.275	0.7275	0.488	0.34	0.39							
S2-S3 linker	R174	D202	S2-S3 linker	0.3175	0.628	0.62	0.453	0.315	0.38							
		D242	S4	0.035	0.123	0.13	0.013	0.155	0.008							
		Q244	S4	0.1375	0.163	0.11	0.135	0.0425	0.253							
	R190	Q357	$S6_{CT}$	0.0075	0.003	0.1825	0	0.0325	0.01							
	R195	D202	S2-S3 linker	0.0575	0.045	0.115	0.275	0.1	0.02							
		D242	S4	0.1125	0.433	0.3775	0.185	0.16	0.083							
	D202	R237	S4	0	0.005	0	0	0	0.498							
		H240	S4	0.5775	0.705	0.6875	0.455	0.57	0.998							
		R243	S4	0.5575	0.498	0.9525	0.655	0.5775	0.353							
		Q244	S4	0.0725	0.035	0.1975	0.04	0.0825	0.253							
S4 helix	R228	D286	S5-P linker	0.2225	0.423	0.715	0.463	0.1075	0.583	R228	E43	NT	0.23	0	0.015	0
	R231	Q234	S4	0.9875	0.988	0.89	0.963	0.63	0.975							
	Q234	R237	S4	0.59	0.423	0.4975	0.438	0.915	0.365							
	H240	D242	S4	0.2925	0.505	0.18	0.408	0.125	0.3							
		Q244	S4	0.175	0.49	0.39	0.473	0.06	0.328							
	D242	R243	S4	0.59	0.648	0.3825	0.683	0.305	0.468							
		R244	S4	0.01	0.043	0.01	0.253	0.01	0.043							
		R249	S4-S5 linker	0.4625	0.43	0.4875	0.08	0.4325	0.36							
	R243	Q244	S4	0.2875	0.063	0.2175	0.268	0.1225	0.103							
	Q244	R249	S4-S5 linker	0.01	0.105	0.05	0.23	0.1	0.003							
	R249	Q260	S4-S5 linker	0	0	0	0.015	0.05	0.213							
		Q357	$S6_{CT}$	0.15	0.01	0	0.003	0.05	0.175							
		Q359	$S6_{CT}$	0.01	0.243	0	0.01	0.08	0.223							
S4-S5 linker	H258	Q260	S4-S5 linker	0.21	0.005	0.11	0	0.04	0.205							
		E261	S4-S5 linker	0.98	0.925	0.94	0.955	0.98	0.83							
		Q356	$S6_{CT}$	0.15	0.36	0.42	0.473	0.15	0.05							
		Q359	$S6_{CT}$	0.01	0.025	0.15	0.135	0.03	0							
	R259	E261	S4-S5 linker	0.05	0.218	0.11	0.175	0.07	0.043							
		Q356	$S6_{CT}$	0.01	0	0.01	0.218	0	0.05							
		Q359	$S6_{CT}$	0.14	0	0.01	0.073	0.03	0.09							
	Q260	E261	S4-S5 linker	0.64	0.635	0.72	0.735	0.74	0.758							
		Q356	$S6_{CT}$	0.4	0.04	0.11	0.143	0.29	0.453							
		Q357	$S6_{CT}$	0.27	0.238	0	0.228	0.14	0.113							
		Q359	$S6_{CT}$	0.29	0.043	0.19	0.123	0.03	0.143							
	E261	Q356	$S6_{CT}$	0.49	0.165	0.35	0.34	0.46	0.48	E261	R67	TMD	0.32	0.1	0.12	0.045
		Q357	$S6_{CT}$	0.16	0.018	0.03	0.178	0.22	0.033							
		Q359	$S6_{CT}$	0.28	0.005	0.38	0.24	0.02	0.06							
S5-P linker	E284	R293	S5-P linker	0	0.015	0	0.02	0	0.253	E284	R32	NT	0	0	0.42	0.415
		Q321	P-S6 linker	0.85	0.898	0.79	0.915	0.69	0.82							
	D286	Q321	P-S6 linker	0.16	0.005	0	0.085	0	0	D286	R32	NT	0	0	0.13	0.01
											R33	NT	0	0	0.04	0.265
											R36	NT	0	0.145	0.58	0
	N289	R293	S5-P linker	0.12	0.005	0.03	0.183	0.18	0.12	N289	Q22	NT	0.03	0.495	0	0
		Q321	P-S6 linker	0.06	0.013	0.7	0.365	0.17	0.395		Q23	NT	0.53	0.305	0	0
											R33	NT	0.45	0.31	0.06	0
											R36	NT	0	0.005	0.12	0
	E290	R293	S5-P linker	0.01	0.025	0.04	0.115	0.03	0.285	E290	Q22	NT	0	0.34	0	0
		Q321	P-S6 linker	0.28	0.055	0.31	0.108	0.38	0.115		R32	NT	0	0	0.65	0.685
											R33	NT	0.1	0.29	0.09	0.02
	R293	E295	S5-P linker	0.05	0.338	0.04	0.29	0.17	0.215	R293	E19	NT	0.4	0.345	0.02	0
		D317	SF	0.01	0.133	0.02	0.283	0.01	0.13		Q22	NT	0.83	0.135	0.16	0
		Q321	P-S6 linker	0.07	0.445	0	0.313	0.1	0.343							
	E295	Q321	P-S6 linker	0.33	0.7	0.87	0.503	0.8	0.75	E295	R32	NT	0	0	0	0.65
P-S6 linker	D317	Q321	P-S6 linker	0.08	0.163	0.09	0.018	0.2	0.185							
										Q321	E19	NT	0.11	0.19	0	0
											Q22	NT	0	0.27	0	0
											Q23	NT	0.36	0.615	0	0
											R32	NT	0	0	0.25	0.245
											E43	NT	0	0.16	0.01	0

a MDS#1: MD simulations with 600 mM [KCl] and +435 mV transmembrane voltage

b MDS#2: MD simulations with 4 K^+ ions in the pore, Cl- ions to neutralize the system, and 0 mV transmembrane voltage

c Q1 domain_1 and Residue_1: The domain and Q1 residue with which Q1 residue_2 or E1_residue form salt-bridge or H-bond with.

d Q1 domain_2 and Residue_2: The domain and Q1 residue that forms salt-bridge or H-bond with Q1 residue_1

e E1 domain and Residue: The domain and E1 residue that forms salt-bridge or H-bond with Q1 residue.

f Frequency: Fraction of 5000 poses during the second half (50-100 ns) MD trajectory in which the specified salt-bridge or H-bond occurre divided by 4 for Q1-Q1 interactions and divided by 2 for Q1-E1 interactions

TABLE S2 KCNE1 Y46 makes extensive contacts with KCNQ1 S1-S2, S5-P and P-S6 linkers

			Q1Ea								Q1Eb							
	Q1 residue[a]	Q1 domain[a]	AE[d]	BE[d]	CE[d]	DE[d]	AF[d]	BF[d]	CF[d]	DF[d]	AE[d]	BE[d]	CE[d]	DE[d]	AF[d]	BF[d]	CF[d]	DF[d]
MDS#1[b]																		
H-B interactions	S140	S1-S2 linker	0	0	0	0	0	0	0	0	0	0	0	0	0.01	0	0	0
	Q147	S1-S2 linker	0	0	0	0	0	0	0	0	0	0	0.09	0	0	0	0	0
	Y148	S1-S2 linker	0	0	0	0	0	0	0	0	0	0	0.01	0	0.19	0	0	0
	S298	S5-P linker	0	0	0	0	0	0	0	0	0	0.19	0	0	0	0	0	0
	D301	S5-P linker	0	0	0	0	0	0	0	0	0	0.01	0	0	0	0	0	0
	W323	P-S6 linker	0	0	0	0	0	0	0.13	0	0.04	0	0	0	0	0	0.05	0
	V324	P-S6 linker	0	0	0	0	0	0	0.24	0	0	0	0	0	0	0	0	0
Hydrophobic interactions	T144	S1-S2 linker	0	0	0	0	0	0	0	0	0	0	0	0	0.31	0	0	0
	Y148	S1-S2 linker	0	0	0	0	0	0	0	0	0	0	0	0	0.12	0	0	0
	A149	S1-S2 linker	0	0	0	0	0	0	0	0	0	0	0	0	0.01	0	0	0
	S298	S5-P linker	0	0	0	0	0	0	0	0	0	0.04	0	0	0	0	0	0
	Y299	S5-P linker	0	0	0	0	0	0	0	0	0	0	0	0	0	0.02	0	0
	A300	S5-P linker	0	0	0	0	0	0	0	0	0	0.33	0	0	0	0.15	0	0
	D301	S5-P linker	0	0	0	0	0	0	0	0	0	0.04	0	0	0	0	0	0
	W323	P-S6 linker	0	0	0	0	0	0	0.38	0	0.27	0	0	0	0	0	0.22	0
	V324	P-S6 linker	0	0	0	0	0	0	0.17	0	0	0	0	0	0	0	0	0
MDS#2[c]																		
H-B interactions	L137	S1-S2 linker	0	0	0.11	0	0	0	0	0	0	0	0	0	0	0	0	0
	S140	S1-S2 linker	0	0	0.06	0	0	0	0	0	0	0	0.01	0	0	0	0	0
	V141	S1-S2 linker	0	0	0.09	0	0.29	0	0	0	0	0	0	0	0	0	0	0
	L142	S1-S2 linker	0	0	0	0	0.03	0	0	0	0	0	0	0	0	0	0	0
	S143	S1-S2 linker	0	0	0	0	0.04	0	0	0	0	0	0	0	0	0	0	0
	T144	S1-S2 linker	0	0	0.06	0	0	0	0	0	0	0	0.03	0	0.04	0	0	0
	Q147	S1-S2 linker	0	0	0	0	0	0	0	0	0	0	0.04	0	0.01	0	0	0
	G297	S5-P linker	0	0	0	0	0	0	0	0	0	0.05	0	0	0	0	0	0
	S298	S5-P linker	0	0	0	0	0	0.01	0	0	0	0.11	0	0	0	0.06	0	0
	Y299	S5-P linker	0	0	0	0	0	0	0	0	0	0	0	0	0	0.09	0	0
	A300	S5-P linker	0	0	0	0	0	0	0	0	0	0.04	0	0	0	0.17	0	0
	D301	S5-P linker	0	0	0	0	0	0	0	0	0	0.26	0	0	0	0.06	0	0
	W323	P-S6 linker	0	0	0	0	0	0	0.04	0	0.04	0	0	0	0	0	0.33	0
Hydrophobic interactions	L137	S1-S2 linker	0	0	0.24	0	0	0	0	0	0	0	0	0	0	0	0	0
	S140	S1-S2 linker	0	0	0.17	0	0	0	0	0	0	0	0.01	0	0	0	0	0
	V141	S1-S2 linker	0	0	0.26	0	0.31	0	0	0	0	0	0	0	0	0	0	0
	L142	S1-S2 linker	0	0	0	0	0.25	0	0	0	0	0	0	0	0	0	0	0
	S143	S1-S2 linker	0	0	0	0	0.01	0	0	0	0	0	0	0	0	0	0	0
	T144	S1-S2 linker	0	0	0	0	0	0	0	0	0	0	0.03	0	0.01	0	0	0
	Q147	S1-S2 linker	0	0	0	0	0	0	0	0	0	0	0.01	0	0	0	0	0
	G297	S5-P linker	0	0	0	0	0	0	0	0	0	0.06	0	0	0	0	0	0
	S298	S5-P linker	0	0	0	0	0	0	0	0	0	0.29	0	0	0	0.03	0	0
	A300	S5-P linker	0	0	0	0	0	0.02	0	0	0	0.47	0	0	0	0.43	0	0
	D301	S5-P linker	0	0	0	0	0	0	0	0	0	0.07	0	0	0	0.01	0	0
	W323	P-S6 linker	0	0	0	0	0	0	0.3	0	0.28	0	0	0	0	0	0.29	0

a. Q1 residue that interacts with Y46 and the Q1 domain

b. MDS#1: MD simulations with 600 mM [KCl] and +435 mV transmembrane voltage

c. MDS#2: MD simulations with 4 K^+ ions in the pore, Cl- ions to neutralize the system, and 0 mV transmembrane voltage

d. The site of interaction is marked by the Q1 subunits (designated as 'A' to 'D'), and the E1 subunits (designated 'E' and 'F').

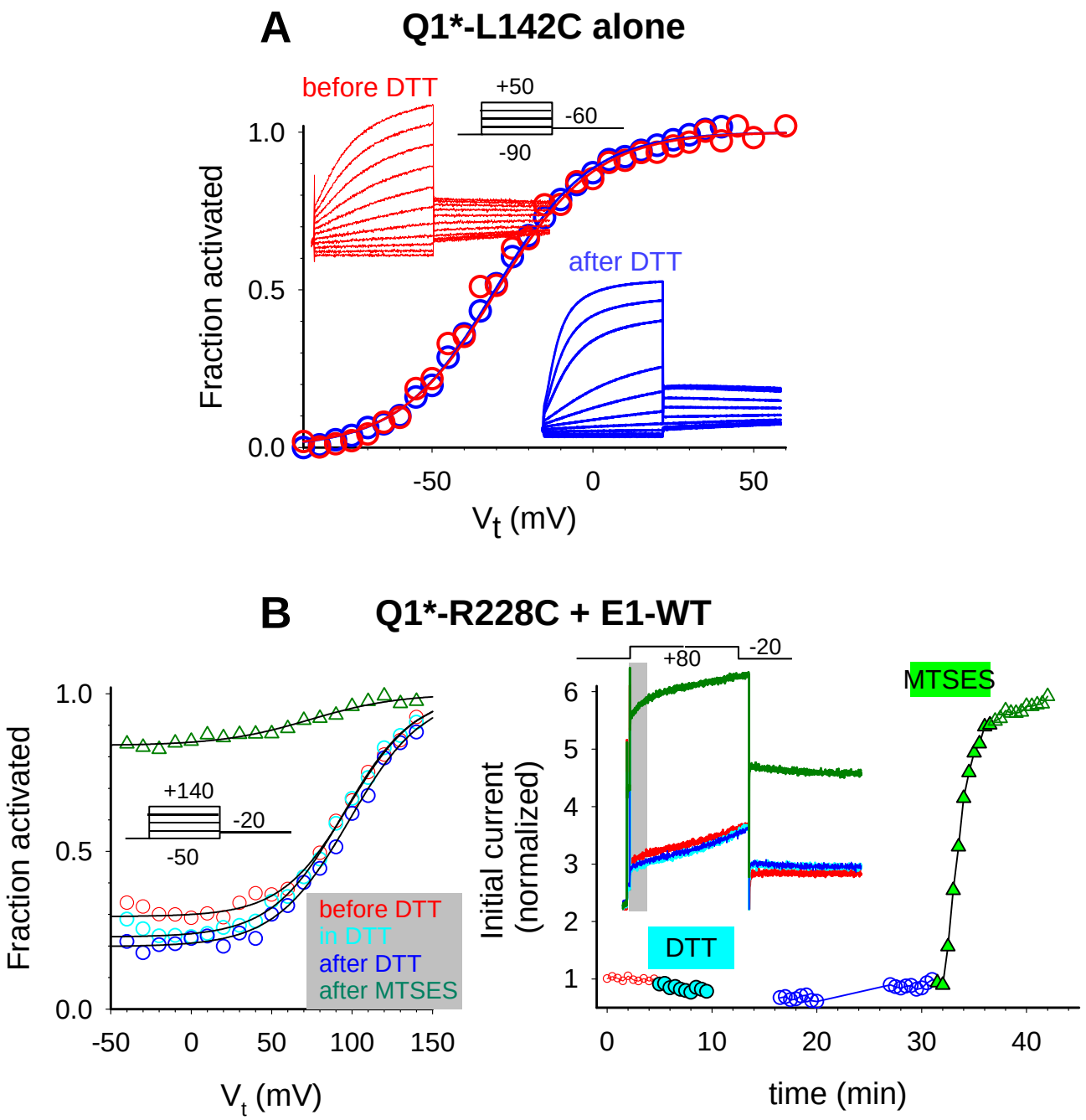
A
Q1*-L142C alone
before DTT
+50
-60
-90
after DTT
Fraction activated
1.0
0.5
0.0
-50
0
50
Vt (mV)
B
Q1*-R228C + E1-WT
+140
-20
-50
before DTT
in DTT
after DTT
after MTSES
Fraction activated
1.0
0.5
0.0
-50
0
50
100
150
Vt (mV)
+80
-20
MTSES
DTT
Initial current (normalized)
6
5
4
3
2
1
0
10
20
30
40
time (min)

Fig. S1

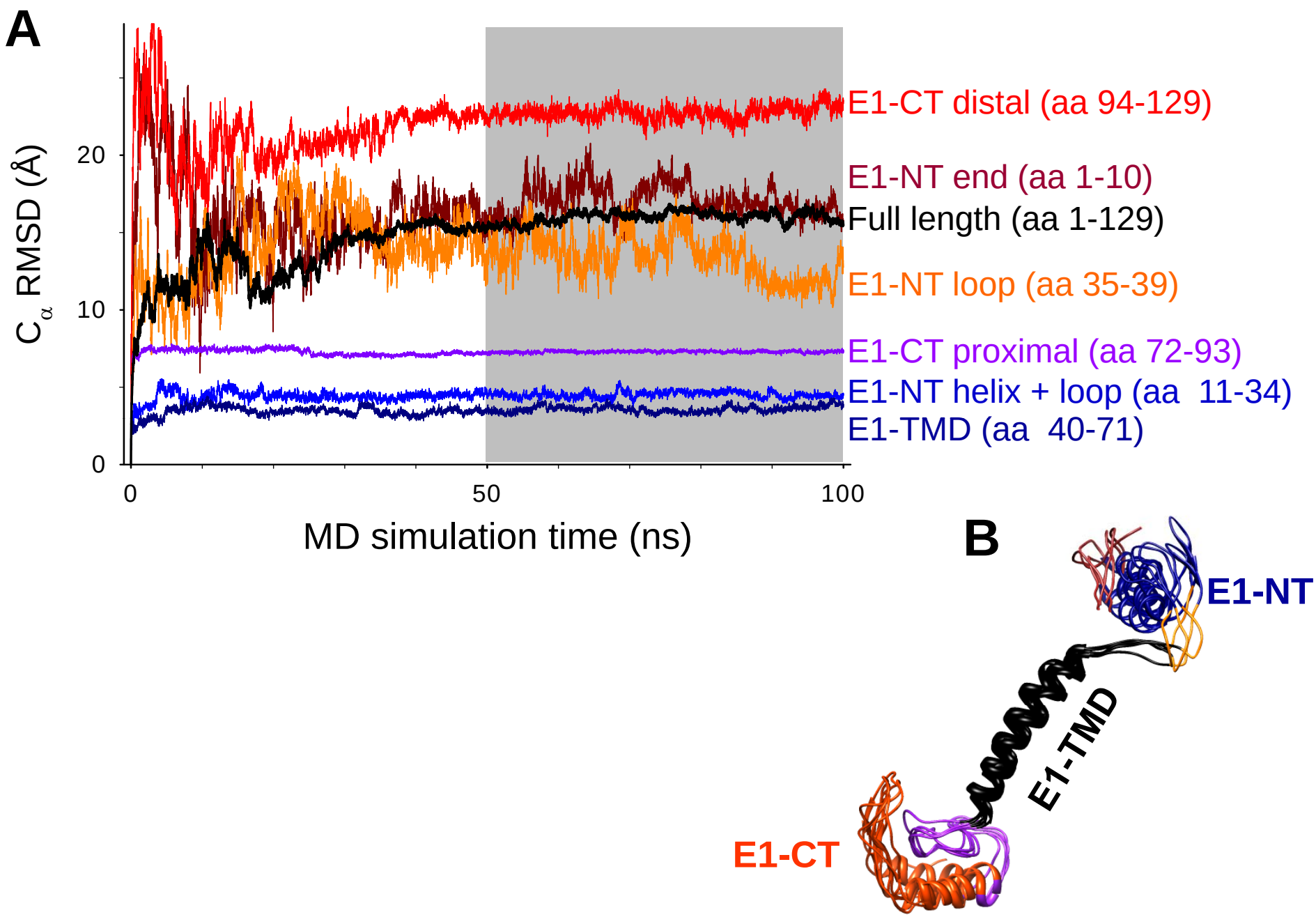
A
C_α RMSD (Å)
0
10
20
0
50
100
MD simulation time (ns)
E1-CT distal (aa 94-129)
E1-NT end (aa 1-10)
Full length (aa 1-129)
E1-NT loop (aa 35-39)
E1-CT proximal (aa 72-93)
E1-NT helix + loop (aa 11-34)
E1-TMD (aa 40-71)
B
E1-NT
E1-TMD
E1-CT

Fig. S2

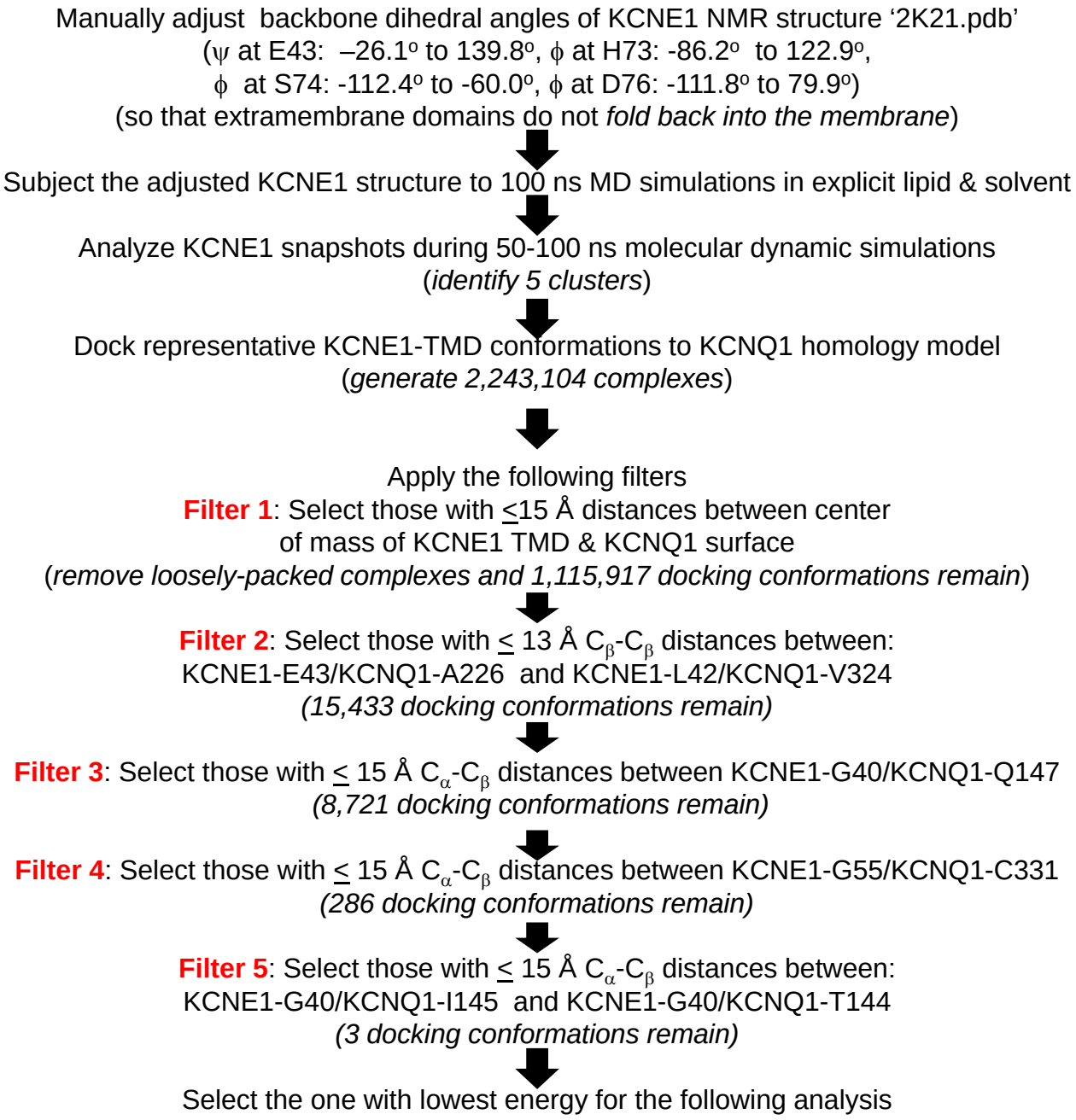
Manually adjust backbone dihedral angles of KCNE1 NMR structure '2K21.pdb'
(ψ at E43: –26.1° to 139.8°, ϕ at H73: -86.2° to 122.9°,
ϕ at S74: -112.4° to -60.0°, ϕ at D76: -111.8° to 79.9°)
(so that extramembrane domains do not *fold back into the membrane*)
Subject the adjusted KCNE1 structure to 100 ns MD simulations in explicit lipid & solvent
Analyze KCNE1 snapshots during 50-100 ns molecular dynamic simulations
(*identify 5 clusters*)
Dock representative KCNE1-TMD conformations to KCNQ1 homology model
(*generate 2,243,104 complexes*)
Apply the following filters
Filter 1: Select those with ≤15 Å distances between center
of mass of KCNE1 TMD & KCNQ1 surface
(*remove loosely-packed complexes and 1,115,917 docking conformations remain*)
Filter 2: Select those with ≤ 13 Å C_β-C_β distances between:
KCNE1-E43/KCNQ1-A226 and KCNE1-L42/KCNQ1-V324
(15,433 docking conformations remain)
Filter 3: Select those with ≤ 15 Å C_α-C_β distances between KCNE1-G40/KCNQ1-Q147
(8,721 docking conformations remain)
Filter 4: Select those with ≤ 15 Å C_α-C_β distances between KCNE1-G55/KCNQ1-C331
(286 docking conformations remain)
Filter 5: Select those with ≤ 15 Å C_α-C_β distances between:
KCNE1-G40/KCNQ1-I145 and KCNE1-G40/KCNQ1-T144
(3 docking conformations remain)
Select the one with lowest energy for the following analysis

Fig. S3

A

Begin with
1 docking conformation of $(Q1)_4$/(E1-TMD) (aa 40-71)
5 clusters of E1-NT (aa 1-34) conformations

↓

Dock 5 representative E1-NT conformations
to $(Q1)_4$/$(E1\text{-}TMD)_4$
(*generate 237,268 conformations*)

↓

Select those with ≤ 15 Å distances between
center of mass of E1-NT & Q1 external surface
(103,818 *conformations remain*)

↓

Select those with ≤ 18 Å distances between
aa 34 of E1-NT & aa 40 of E1-TMD
(*30,254 conformations remain*)

↓

Substitute $(Q1)_4$ with ChTx/$(Q1^s)_4$ to generate
ChTx/$(Q1^s)_4$/$(E1\text{-}TMD)_4$/(E1-NT)

↓

Filter 1: Select those with C_α-C_α distances ≤ 18 Å
between E1 positions 14 & 34
& ChTx position 19
(*916 conformations remain*)

↓

Filter 2: Remove those having clashes between
E1-NT & ChTx

↓

Filter 3: Remove those with similar configurations
(C_α-C_α RMSD ≤ 3.5 Å)
(22 *conformations remain, see panel D,*
classified into 4 groups: R1Ea, R2Ea, R1Eb, R2Eb)

↓

Filter 4: Remove those with the following issues:
1. N-glycosylation sites (N5 & N26) buried
2. E1 positions 14, 22 and/or 34 face way
or are blocked from Q1 pore entrance
3. LQT5 mutation site residues (A8, T10, R32)
far from Q1 external surface

↓

Four conformations remain
(2 in R2Ea group, 2 in R1Eb group)
Select one from each group

→

Build the loop between E1-NT & E1-TMD
(aa 35-39)

↑

Remove ChTx & extra E1-TMD, replace $Q1^s$ with
WT Q1, duplicate E1-TMD-NT
to create 2 versions of $(Q1)_4$/$(E1\text{-}TMD\text{-}NT)_2$:
Q1/Ea & Q1/Eb

↑

Subject Q1/Ea & Q1/Eb to 100-ns MD simulations
in POPC lipid bilayer & explicit solvent

C

Color code
ChTx
Q1 chains:
A, B, C, D

Highlighted:
interacting
ChTx/Q1
residues

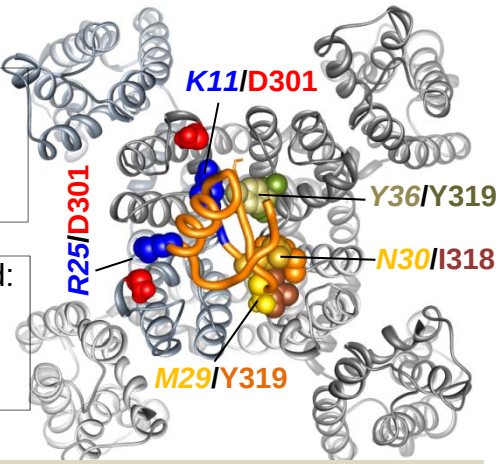

B

Begin with:
NMR structure of ChTx docked to $KcsA^s$

↓

Substitute $KcsA^s$ with $Q1^s$ & confirm
expected contacts between ChTx & $Q1^s$

↓

Generate 1 ChTx/$(Q1^s)_4$ conformation
(see panel C)

D

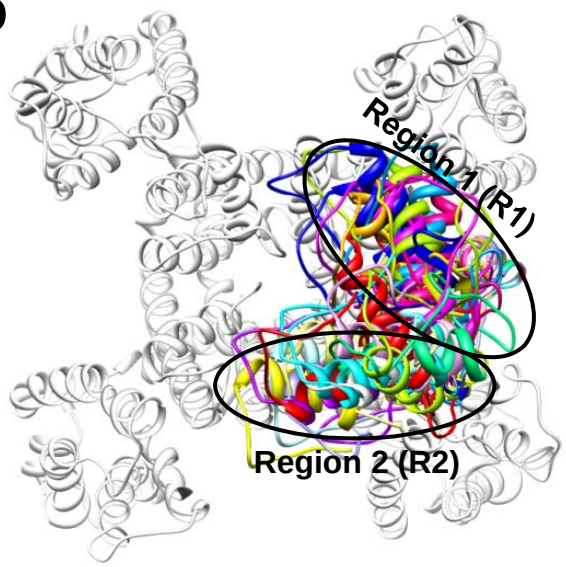

Fig. S4

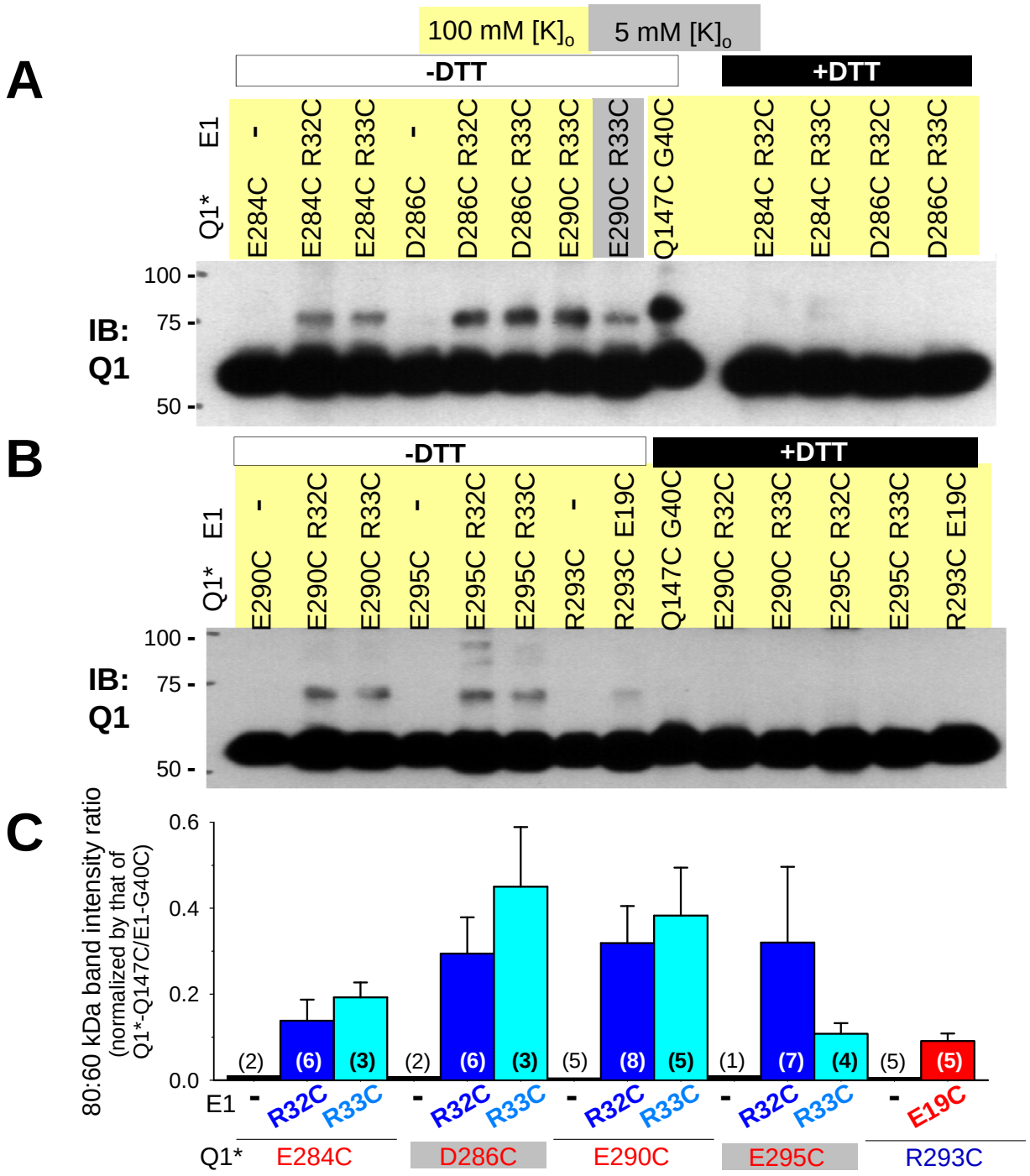
A
100 mM [K]o
5 mM [K]o
-DTT
+DTT
E1
Q1*
-
E284C R32C
E284C R33C
D286C R32C
D286C R33C
E290C R33C
Q147C G40C
E284C R32C
E284C R33C
D286C R32C
D286C R33C
100
75
50
IB:
Q1
B
-DTT
+DTT
E1
Q1*
-
E290C R32C
E290C R33C
E295C R32C
E295C R33C
R293C E19C
Q147C G40C
E290C R32C
E290C R33C
E295C R32C
E295C R33C
R293C E19C
100
75
50
IB:
Q1
C
80:60 kDa band intensity ratio
(normalized by that of
Q1*-Q147C/E1-G40C)
0.6
0.4
0.2
0.0
(2) (6) (3) (2) (6) (3) (5) (8) (5) (1) (7) (4) (5) (5)
E1 - R32C R33C - R32C R33C - R32C R33C - R32C R33C - E19C
Q1* E284C D286C E290C E295C R293C

Fig. S5

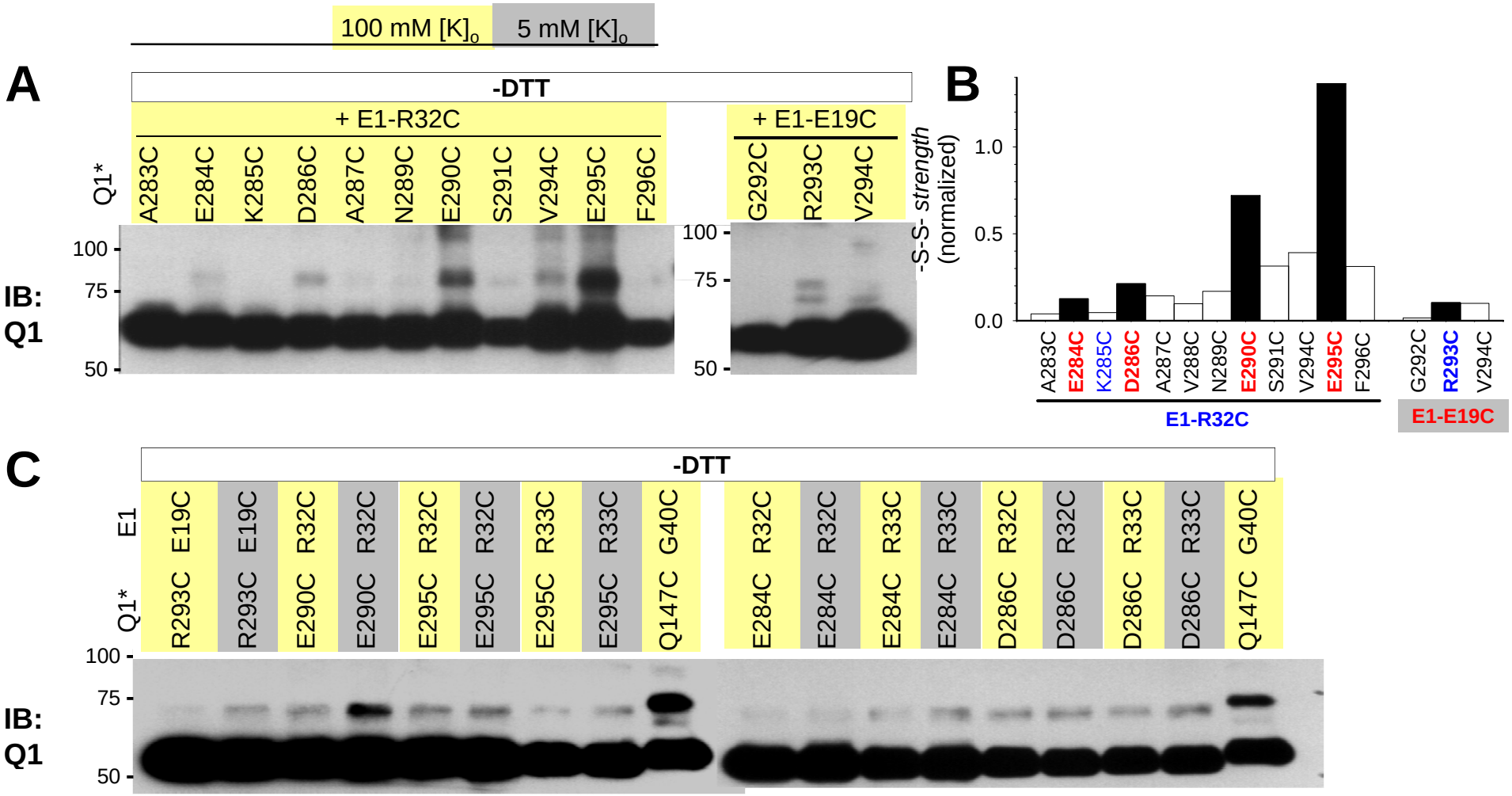
100 mM [K]o
5 mM [K]o
A
-DTT
+ E1-R32C
+ E1-E19C
Q1*
A283C
E284C
K285C
D286C
A287C
N289C
E290C
S291C
V294C
E295C
F296C
G292C
R293C
V294C
IB:
Q1
100
75
50
B
-S-S- strength
(normalized)
1.0
0.5
0.0
A283C
E284C
K285C
D286C
A287C
V288C
N289C
E290C
S291C
V294C
E295C
F296C
G292C
R293C
V294C
E1-R32C
E1-E19C
C
-DTT
E1
Q1*
E19C
R293C
R32C
E290C
E295C
R33C
Q147C
G40C
E284C
D286C

Fig. S6

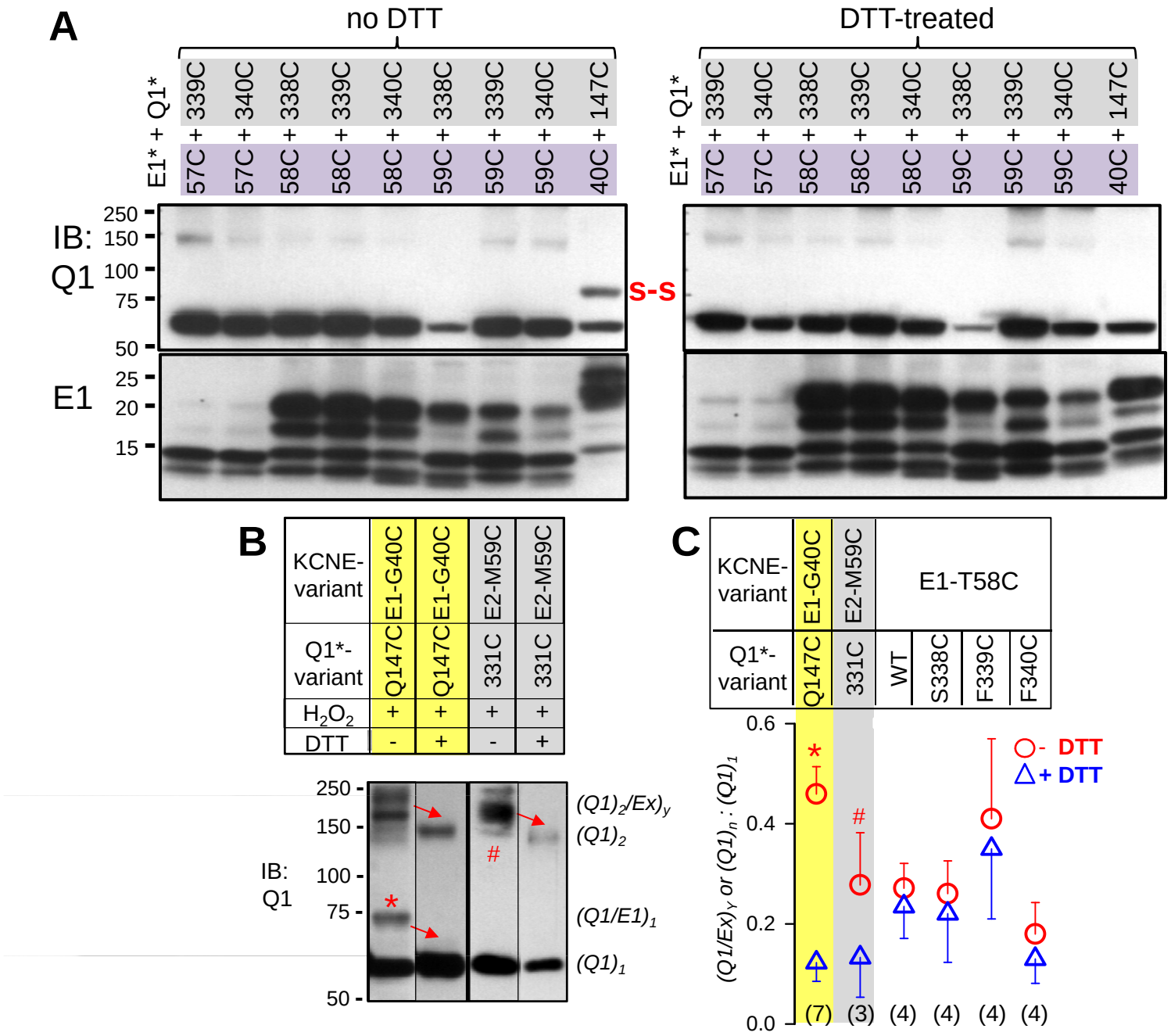
A
no DTT
DTT-treated
E1* + Q1*
339C + 57C
340C + 57C
338C + 58C
339C + 58C
340C + 58C
338C + 59C
339C + 59C
340C + 59C
147C + 40C
IB: Q1
E1
250
150
100
75
50
25
20
15
S-S
B
KCNE-variant
E1-G40C
E2-M59C
Q1*-variant
Q147C
331C
H2O2
DTT
IB: Q1
(Q1)2/Ex)y
(Q1)2
(Q1/E1)1
(Q1)1
C
E1-T58C
WT
S338C
F339C
F340C
(Q1/Ex)y or (Q1)n : (Q1)1
0.6
0.4
0.2
0.0
- DTT
+ DTT
(7)
(3)
(4)
(4)
(4)
(4)

Fig. S7

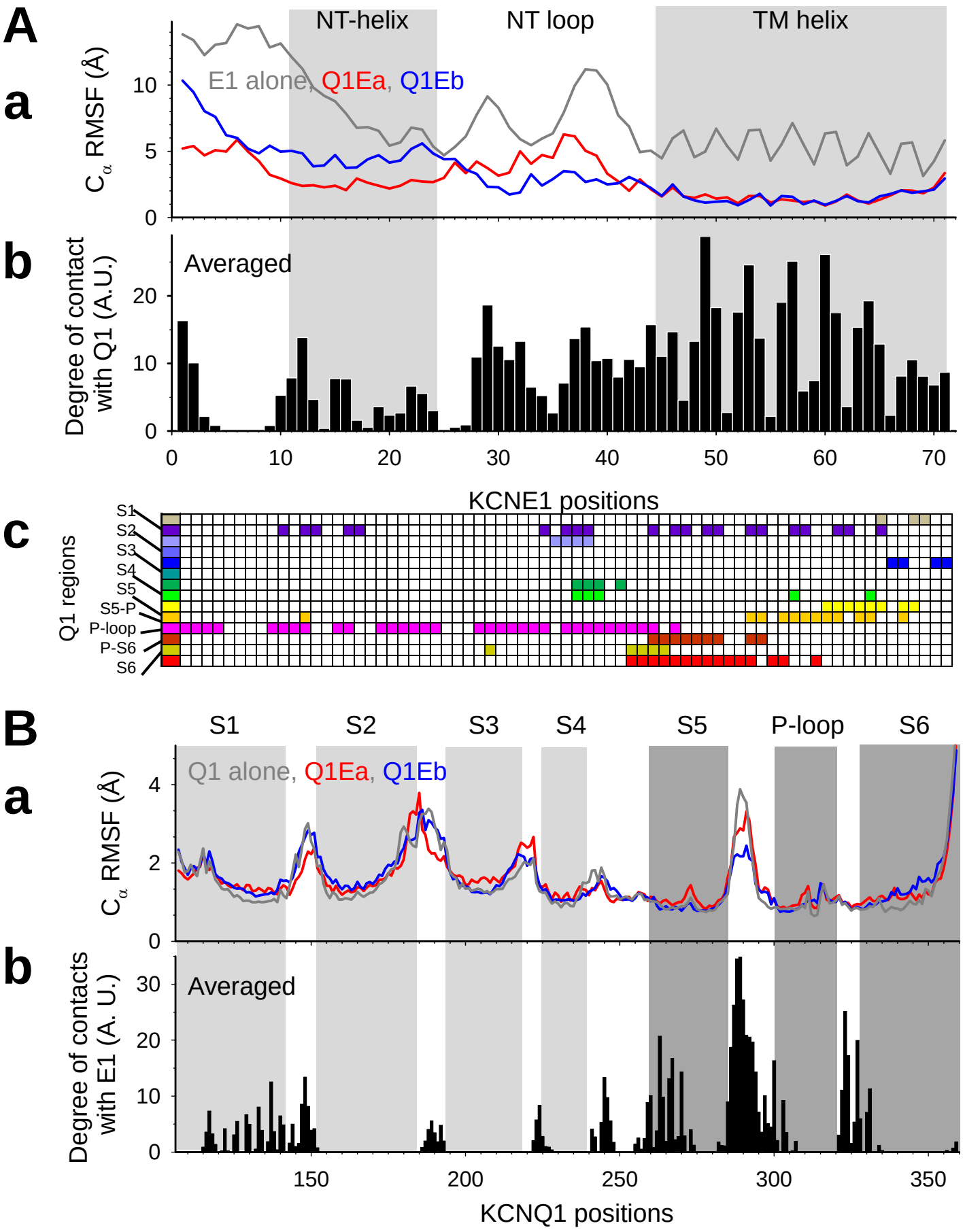
A
a
NT-helix
NT loop
TM helix
E1 alone, Q1Ea, Q1Eb
C_α RMSF (Å)
b
Averaged
Degree of contact with Q1 (A.U.)
KCNE1 positions
c
Q1 regions
S1
S2
S3
S4
S5
S5-P
P-loop
P-S6
S6
B
a
S1
S2
S3
S4
S5
P-loop
S6
Q1 alone, Q1Ea, Q1Eb
C_α RMSF (Å)
b
Averaged
Degree of contacts with E1 (A. U.)
KCNQ1 positions

Fig. S8

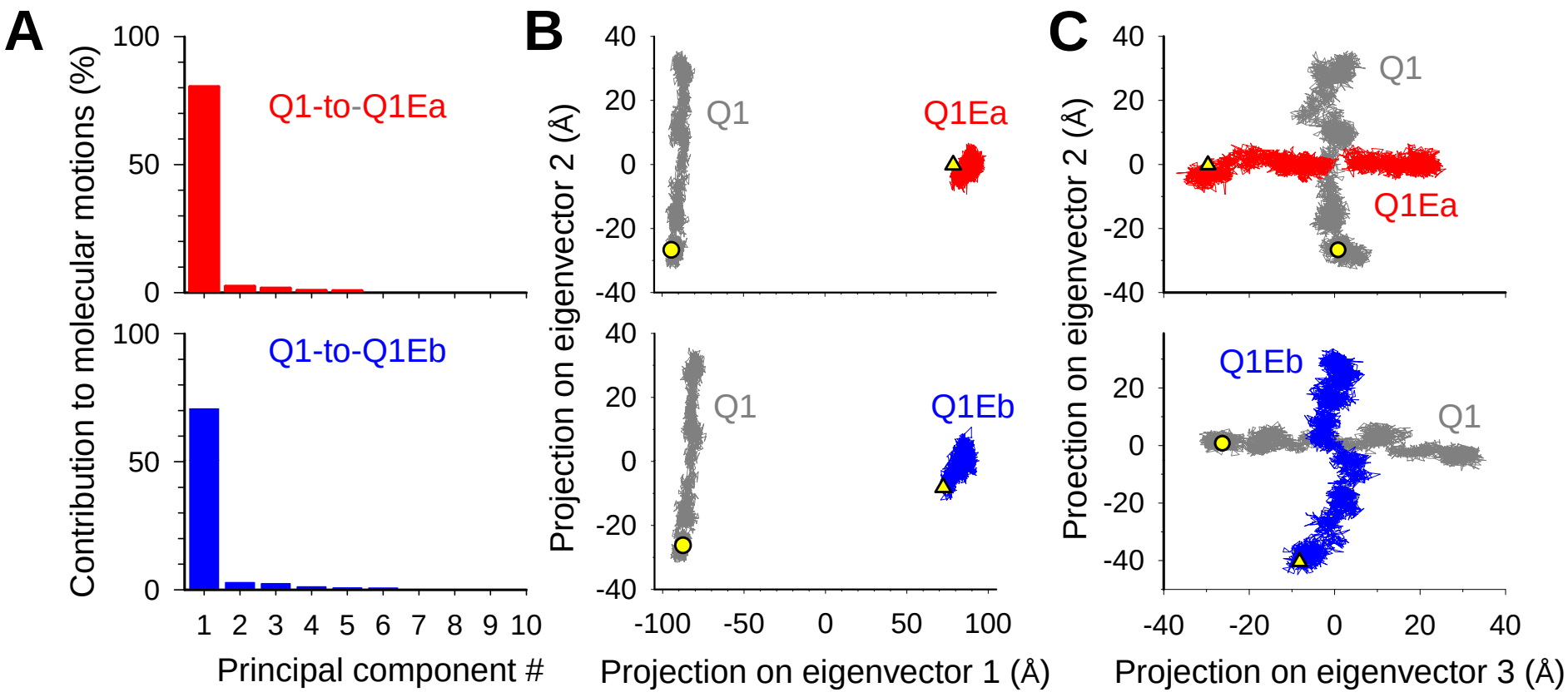
A
B
C
Contribution to molecular motions (%)
Q1-to-Q1Ea
Q1-to-Q1Eb
Principal component #
Projection on eigenvector 2 (Å)
Q1
Q1Ea
Q1Eb
Projection on eigenvector 1 (Å)
Proection on eigenvector 2 (Å)
Projection on eigenvector 3 (Å)

Fig. S9

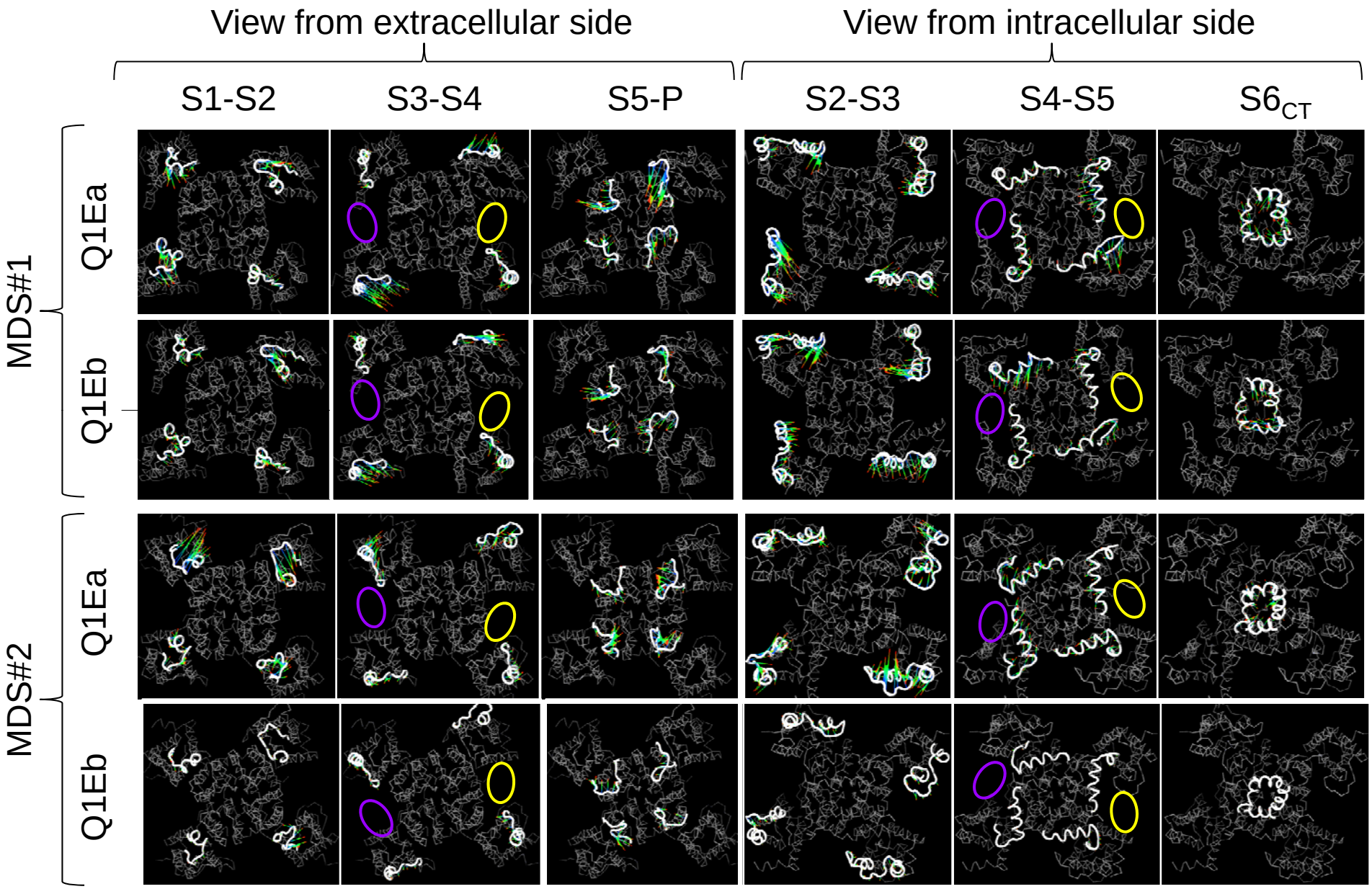
View from extracellular side
View from intracellular side
S1-S2
S3-S4
S5-P
S2-S3
S4-S5
S6CT
MDS#1
Q1Ea
Q1Eb
MDS#2
Q1Ea
Q1Eb

Fig. S10

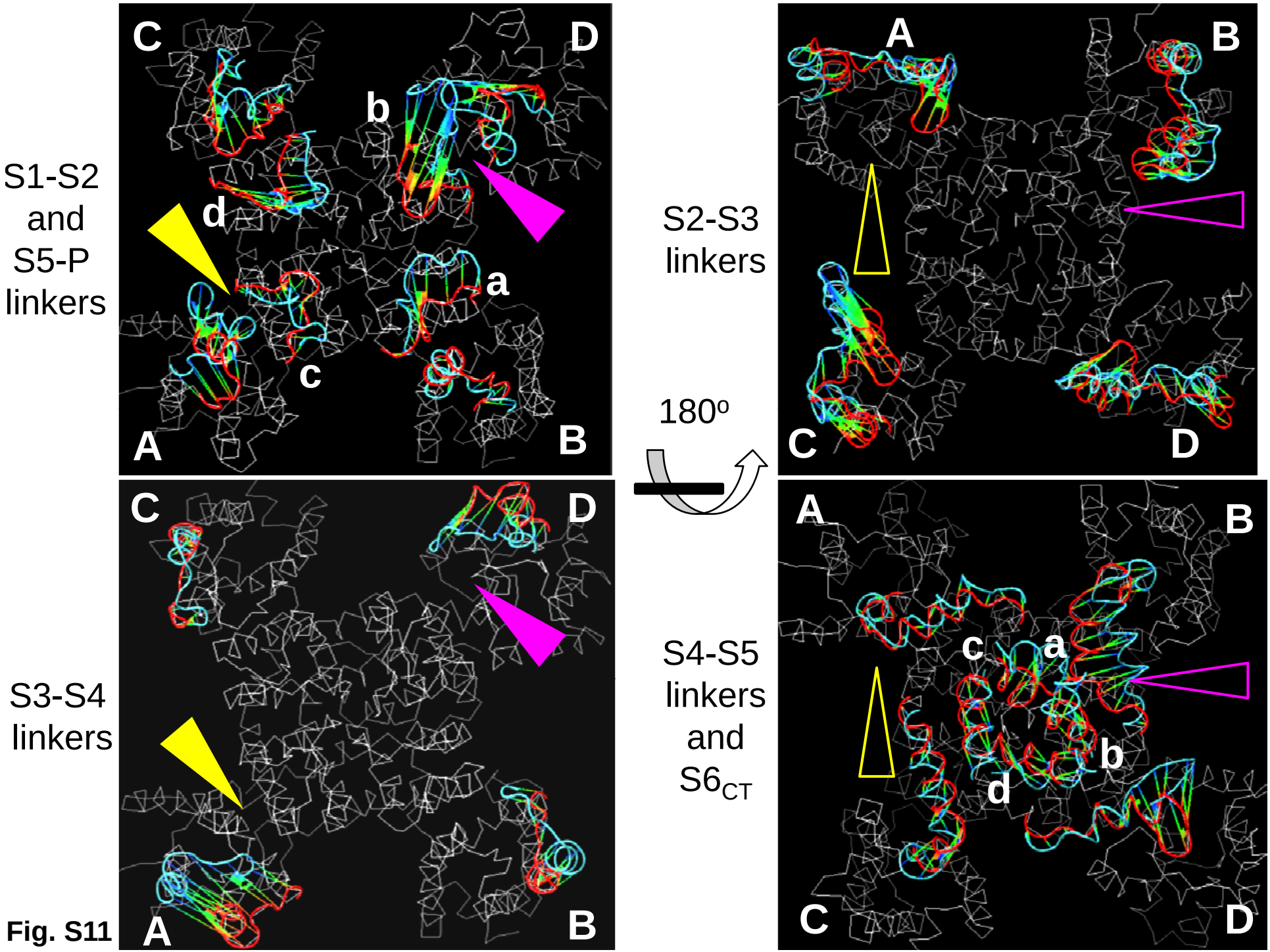
S1-S2
and
S5-P
linkers
C
D
b
d
a
c
A
B
S2-S3
linkers
A
B
180º
C
D
S3-S4
linkers
C
D
A
B
S4-S5
linkers
and
S6CT
A
B
c
a
b
d
C
D

Fig. S11

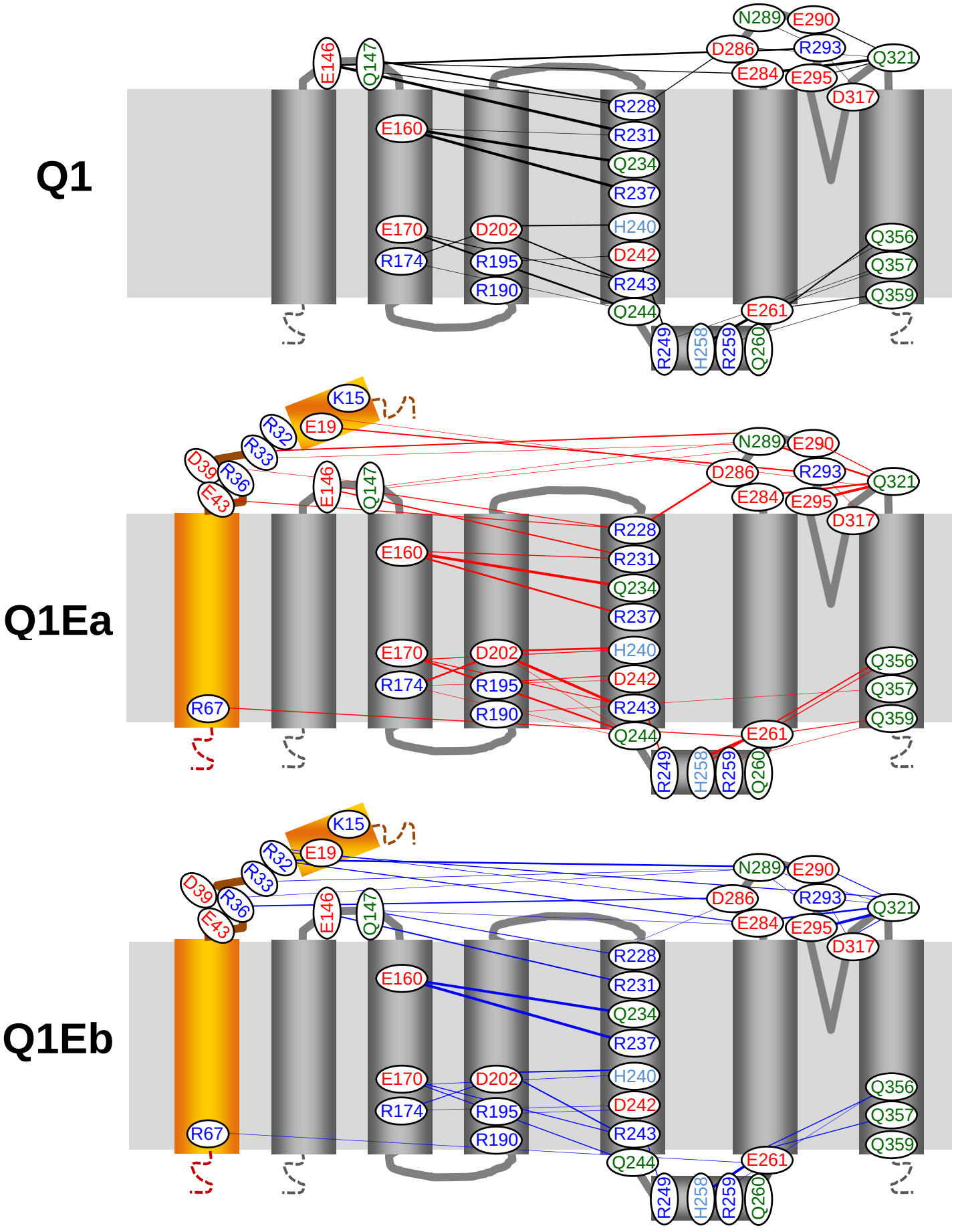
Q1
N289
E290
D286
R293
Q321
E284
E295
D317
E146
Q147
R228
R231
E160
Q234
R237
E170
D202
H240
Q356
R174
R195
D242
Q357
R243
R190
Q359
Q244
E261
R249
H258
R259
Q260
Q1Ea
K15
E19
R32
R33
D39
R36
E43
R67
Q1Eb

Fig. S12

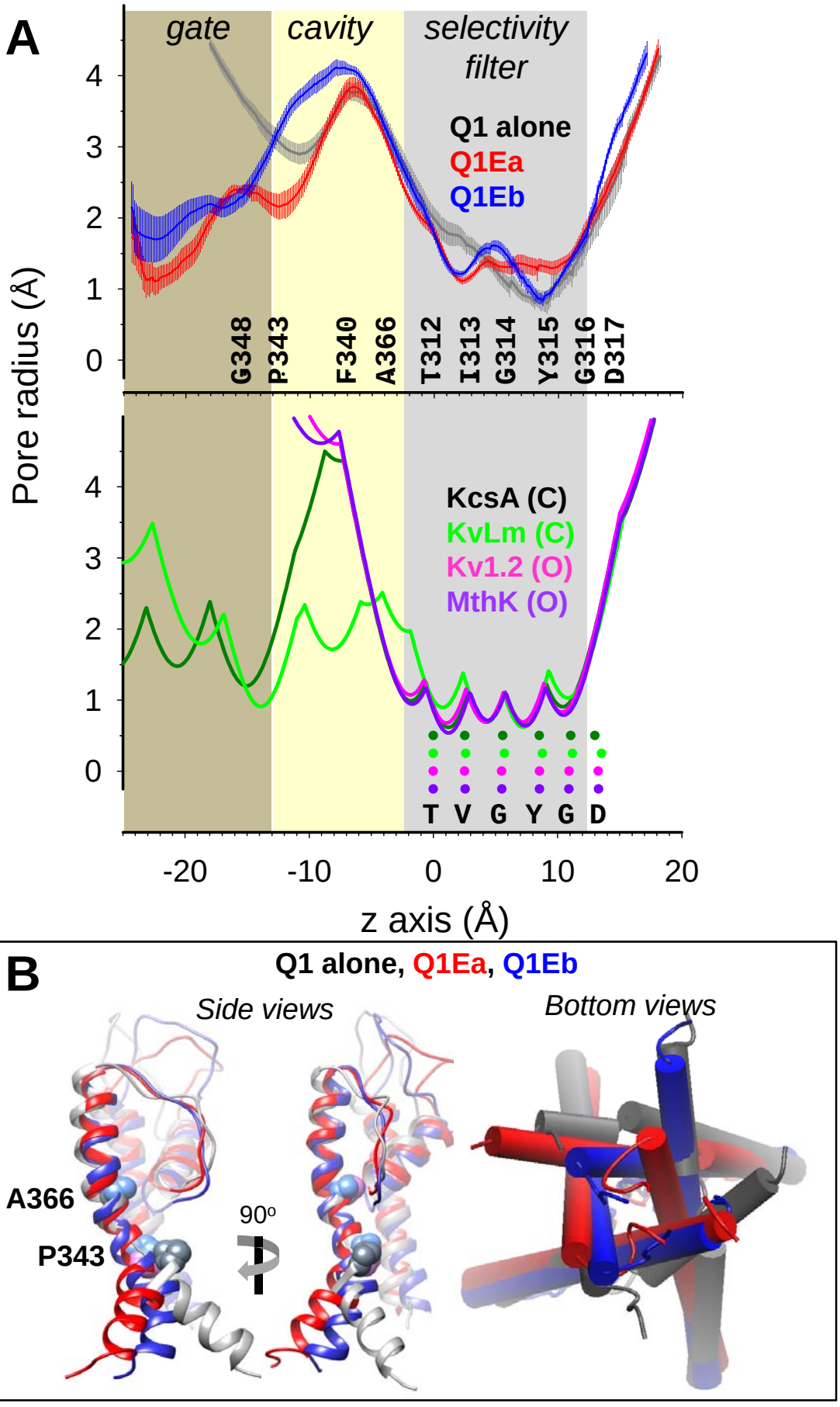
A
gate
cavity
selectivity filter
Q1 alone
Q1Ea
Q1Eb
G348
P343
F340
A366
T312
I313
G314
Y315
G316
D317
KcsA (C)
KvLm (C)
Kv1.2 (O)
MthK (O)
T V G Y G D
Pore radius (Å)
z axis (Å)
B
Q1 alone, Q1Ea, Q1Eb
Side views
Bottom views
A366
P343
90°

Fig. S13